Millimeter, Microwave, Hard X–ray and Soft X–ray Observations of Energetic Electron Populations in Solar Flares

M. R. Kundu[1], S. M. White[1], N. Gopalswamy[1] and J. Lim[1,2]

[1]*Dept. of Astronomy, Univ. of Maryland, College Park MD 20742*

[2]*Solar Astronomy 264–33, Caltech, Pasadena CA 91125*

Submitted to the **Astrophysical Journal Supplement**, *1993 March*

Presented at IAU Colloquium 142, College Park, 1993 January

Received 1993 March 25; revised, 1993 June 1

Abstract

We present comparisons of multi–wavelength data for a number of solar flares observed during the major campaign of 1991 June. The different wavelengths are diagnostics of energetic electrons in different energy ranges: soft X–rays are produced by electrons with energies typically below 10 keV, hard X–rays by electrons with energies in the range 10 – 200 keV, microwaves by electrons in the range 100 keV – 1 MeV, and millimeter–wavelength emission by electrons with energies of 0.5 MeV and above. The flares in the June 1991 active period were remarkable in two ways: all have very high turnover frequencies in their microwave spectra, and very soft hard–X–ray spectra. The sensitivity of the microwave and millimeter data permit us to study the more energetic (> 0.3 MeV) electrons even in small flares, where their high–energy bremsstrahlung is too weak for present detectors. The millimeter data show delays in the onset of emission with respect to the emissions associated with lower–energy electrons and differences in time profiles, energy spectral indices incompatible with those implied by the hard X–ray data, and a range of variability of the peak flux in the impulsive phase when compared with the peak hard X–ray flux which is two orders of magnitude larger than the corresponding variability in the peak microwave flux. All these results suggest that the hard–X–ray–emitting electrons and those at higher energies which produce millimeter emission must be regarded as separate populations. This has implications for the well–known “number problem” found previously when comparing the numbers of nonthermal electrons required to produce the hard X–ray and radio emissions.

Subject headings: Sun: flares; radio radiation; X-rays, gamma rays

1. INTRODUCTION

In 1991 June a major active region appeared on the Sun and proceeded to produce 6 of the largest solar flares ever recorded. An international campaign to carry out coordinated observations of the flares from this region was organized. The millimeter–wavelength interferometer at Hat Creek, operated by the Universities of California at Berkeley, Illinois and Maryland (BIMA), participated in the campaign by observing the Sun for 5 days. The launch of the *Compton Gamma Ray Observatory* earlier in 1991 afforded us our first opportunity to compare the sensitive millimeter–interferometer diagnostic of high–energy electrons with the hard X–ray bremsstrahlung also produced by energetic electrons. In this paper we examine eight separate flares from this period and carry out comparisons at a number of wavelengths. These comparisons are used to study the population of accelerated electrons in a number of different energy ranges, and to try to determine the relationships between them.

Millimeter-wavelength emission from solar flares is of great interest as a complement to space-based γ–ray observations because it arises from the same electrons which produce the γ–rays: electrons with energies above about 1 MeV. This is a consequence of the range of magnetic field strengths in the corona, which requires that any gyrosynchrotron emission at millimeter wavelengths must occur at high harmonics of the gyrofrequency and so can only be produced by electrons with Lorentz factors much greater than unity (White & Kundu 1992). Since high-resolution imaging at gamma-ray energies is not presently possible, millimeter observations can act as a substitute. By contrast, the γ–ray observations are capable of excellent energy spectral discrimination which is difficult to achieve with broadband radio observations. In addition, the millimetric emission is undoubtedly optically thin (except possibly for a small class of very large flares which have spectra rising beyond 100 GHz; Kaufmann *et al.* 1985), and thus is not subject to the same ambiguities of interpretation which are prevalent in the study of solar microwave bursts. It can be used as a powerful diagnostic of the energy distribution of electrons in solar flares and its evolution, and of the magnetic field. Most millimeter-wave observations of solar flares have been hampered both by poor spatial resolution (because of the lack of synthesis interferometers) and by poor sensitivity (since the flux from the Sun's thermal emission is so high at millimeter wavelengths). The number of reported observations of bursts at millimeter wavelengths is relatively small, and there are none for which true high-spatial-resolution imaging data have been reported (see review in White & Kundu 1992).

We have carried out high-spatial-resolution millimeter observations of solar flares using the Berkeley-Illinois-Maryland Array (BIMA). At the present time BIMA consists of only three elements, which is not adequate for mapping highly variable solar phenomena, but is excellent for studies of the temporal structure of flares at millimeter wavelengths at several different spatial scales (Kundu et al. 1990; White et al. 1992; Lim et al. 1992; White & Kundu 1992). In this paper, we present BIMA observations made during the Max '91 Campaign in June 1991 when solar activity was unusually high. Our observations on June 8 – June 13, 1991 occurred during the period June 4–June 15 when the *Compton Gamma Ray Observatory* made the Sun a target of opportunity because of the high level of solar activity. The millimeter data are a diagnostic of the MeV–energy electrons accelerated in flares and the hard X–ray data are a diagnostic of the $\sim$ 25 – 100 keV energy electrons. To fill in the energy spectrum as much as possible, we have also acquired microwave patrol data, which are generally regarded as a diagnostic of electrons with energies of several hundred keV and up; and soft X–ray data, which are diagnostics of plasma at energies below 10 keV. The important feature of the millimeter observations is that they are

much more sensitive than are γ–ray observations to the MeV electron energy range, and thus permit us to study MeV–energy electrons even in small flares, where hard X–rays are barely detected. We present several examples of this below. In the following section we describe the sources of data, and their use as diagnostics of particular energy ranges. Then we present the data for eight flares observed in the 1991 June period, ranging in size from GOES soft X–ray class B1 to M7. Some general conclusions from comparison of the different data are then drawn, and we discuss their implications for electron acceleration during solar flares.

2. SOURCES OF DATA

2.1. Millimeter wavelength data

The millimeter data were obtained with the Berkeley–Illinois–Maryland Array (BIMA) at Hat Creek, CA. The telescope consisted of 3 6–m dishes operating as an interferometer. The use of this telescope for solar observations is described by White & Kundu (1992). The data consist of amplitudes and phases measured for each of the three interferometer pairs every 0.4 seconds. Two sidebands are received (86 and 89 GHz), but there were no significant differences between the sidebands and we will only present data for one in the following. The data were calibrated in amplitude by observations of a point source of known flux every hour.

The antennas were at stations 80E, 0 and 40W, where the designations indicate feet from the array center in the appropriate direction. This gives east–west baselines of 12.2, 24.4 and 36.6 meters, corresponding to interferometer fringe spacings of 59″, 29″ and 20″ as the Sun crossed the meridian during June. The output of the interferometer is the one–dimensional spatial Fourier transform of the brightness distribution in the 2.3′ (at the half–power point) field of view with a wavelength on the sky equal to the fringe spacing; if the brightness is dominated by a source of dimension much smaller than the fringe spacing, the measured amplitude is the flux of the source. The projection of all baselines on the sky is predominantly east–west throughout the day, i.e., the observations are insensitive to the spatial dimension of 86 GHz sources in the north–south direction. Wind problems were experienced with antenna 3 due to its lack of a backlash system, and this caused many dropouts, particularly during afternoon observations (after 22 UT for these observations). For this reason we usually display data from baseline 12, which was relatively unaffected by wind problems, although baseline 23 generally showed the largest flux.

From these data we can extract two pieces of information on source sizes. The first may be obtained from the three measured amplitudes, together with the assumption of a gaussian source shape. Then for the one–dimensional data available here we may fit the relative amplitudes on the three baselines to a gaussian, knowing the fringe spacings, and determine the peak flux of the source and the dimension in one orientation. This technique will not be used quantitatively here because it requires that the relative calibration of the different baselines be well determined, which we did not attempt for these observations; however, it may be used qualitatively, since if the three amplitudes are all similar the source is presumably unresolved on all baselines. The second technique is phase closure: one forms the sum of the phases measured on each of the three baselines, which is a quantity independent of antenna–dependent effects such as atmospheric phase changes. If this quantity is zero, then the source is either effectively a point source for these fringe spacings, or else appears symmetric on the sky about the peak (in this case the east–west baselines mean that the source only needs to be symmetric in an east–west direction). Examples of the application of this technique to BIMA data are given by White & Kundu (1992).

As discussed by White & Kundu (1992), millimeter emission in the impulsive phase of flares is primarily a diagnostic of electrons with MeV energies. The typical gyrofrequency in the corona is several GHz, requiring that emission at 86 GHz is at high harmonics. Electrons with relativistic Lorentz factors less than 2 provide essentially no opacity at these high harmonics. Because it lacks high–energy electrons, a thermal energy spectrum, even with a temperature as high as 10^9 K, produces no gyrosynchrotron emission at millimeter wavelengths. Hot dense plasma does produce thermal free–free emission at millimeter wavelengths, and this is also detected in these observations. We note that an interferometer is not sensitive to sources of dimension larger than about one-third of the fringe spacing, i.e., 20″ – 30″, and thus we are probably not detecting all the thermal free–free flux associated with the post–flare decay in the millimeter observations.

2.2. Hard X–ray/γ–ray data

The data to be used in this study are obtained from the four discriminator channels of the large-area detectors of the Burst And Transient Source Experiment (BATSE; principal investigator, Gerry Fishman, NASA/MSFC) on the *Compton Gamma Ray Observatory* (CGRO). There is such a detector at each of the eight corners of the spacecraft, and solar bursts are identified by determining a direction based on the relative count rates in the different detectors. The discriminator data (DISCLA) consist of 1.024 second accumulations in energy channels with the nominal ranges 25 – 50 keV, 50 – 100 keV, 100 – 300 keV and 300 keV – 1.0 MeV. Each detector has an area of 2000 cm^2 (the effective area for a given flare is reduced by projection onto the Sun–Earth line), making this the most sensitive detector in this energy range ever flown. As we show below, these detectors are easily capable of detecting flares as small as B1 in the GOES soft–X–ray classification scheme.

With the kind cooperation of the BATSE team the raw DISCLA data are being passed immediately to NASA/GSFC where the *Solar Maximum Mission* HXRBS team (principal investigators: Brian Dennis and Richard Schwartz), with the support of the CGRO Guest Investigator program, processes them, identifies solar flares, and maintains a catalog and flare data base. This data base is accessible to the solar community, and we have used it to obtain the data used here. Using the catalog we were able to identify 12 flares observed both by BIMA and by CGRO. Two of these were the > X10 flares of June 9 and June 11; two other flares have spectroscopic data from both BATSE and the Oriented Scintillation Spectrometer Experiment (OSSE) on CGRO, and will be discussed elsewhere (**?**). In this paper we discuss the remaining eight flares.

In this paper we will adopt the usual assumption that the hard X–rays arise from energetic electrons with a power–law energy distribution precipitating from the solar corona into the chromosphere and radiating bremsstrahlung X–rays in collisions with chromospheric material ("thick target" assumption). We have no evidence that in any of the flares to be studied the major contribution to the hard X–rays is from thin–target coronal sources. The properties of thick–target bremsstrahlung mean that hard X–rays (HXR) of energy ϵ are a diagnostic of electrons with energies up to roughly 3ϵ (Kosugi, Dennis & Kai 1988). In our case this will mean that the HXR data are produced typically by electrons with energies below 200 keV.

Although the broadband spectral data obtained from the DISCLA detectors are not really suitable for spectral analysis, we are interested in estimating the energy distribution of the electrons producing the hard X–rays and this can still be done with low precision using these data. We have used a program written by Richard Schwartz (STX/GSFC) specifically to calculate the response of the BATSE detectors to a given input photon spectrum, assuming that the 4 channels have exactly their nominal energy ranges. This program includes the effects of photoelectric

interactions, backscattering, Compton scattering, the K-escape process and the response of the detectors. We calculated channel ratios for input photon spectra ranging from spectral indices γ of –2 to –10, fit the curves with suitable functions and then used the observed channel ratios in the data for the 8 flares to estimate the input photon spectral indices. Where there were sufficient counts, we calculated the spectral index as a function of time through the event. In nearly all cases discussed here, there were insufficient photons above 100 keV to use the higher channel ratios, and all the spectral indices referred to are derived from the ratio of the 25–50 keV channel to the 50–100 keV channel. To calculate an energy spectral index δ for comparison with that to be derived for the radio data, we have assumed that the emission is thick target and accordingly have added 1.5 to the photon spectral index γ to obtain the energy spectral index (the electron flux incident at the chromosphere has an energy spectrum $\delta' = \gamma + 1$ as shown by Brown 1971, and there is a factor of velocity in converting electron flux to number density which gives $\delta = \gamma + 1.5$ in the nonrelativistic limit where $v \propto \sqrt{E}$; e.g., see Kosugi Dennis and Kai 1988). The derived energy distributions were all very soft, and we discuss this point further below.

2.3. Microwave data

To complement the millimeter and hard X-ray data we requested the microwave patrol data from the Radio Solar Telescope Network (RSTN) of telescopes maintained by the Air Force weather service; the data were provided by the National Geophysical Data Center in Boulder (courtesy of G. Deuel). The data are full–disk fluxes at 8 frequencies from 0.24 to 15.4 GHz; here we will only use the two highest frequencies, 8.8 and 15.4 GHz. The time resolution of these data is 1.0 s.

Microwaves in the impulsive phase of solar flares are generally assumed to be due to gyrosynchrotron emission by energetic electrons in the solar corona with a power–law energy distribution. (Here we do not consider thermal gyrosynchrotron emission, since as discussed above the detection of impulsive emission at millimeter wavelengths rules out a thermal energy distribution for the electrons.) The turnover frequency in the radio spectrum of solar flares typically lies in the microwave range: at frequencies below the turnover the radio source is optically thick, the flux spectrum rises with frequency and one only sees down to the optically–thick surface, while at frequencies above the turnover the source is optically thin, one sees contributions from all electrons present, and the flux spectrum falls as frequency increases.

Gyrosynchrotron theory suggests that microwave emission on the optically–thin side of the spectrum ought to be dominated by electrons with energies in excess of 300 keV (Takakura 1967; Ramaty 1969; Holt & Ramaty 1969; Takakura 1972; Dulk & Marsh 1982), while at optically thick frequencies the main contribution arises from somewhat lower–energy electrons. The latter result follows since spatially resolved observations indicate brightness temperatures typically of order 10^8 –10^9 K, which correspond to electrons of energy of order 10 – 100 keV. However, comparisons of microwave and hard X–ray time profiles carried out in the 1980's suggested that in fact even at 17 GHz, which was well on the optically–thin side of the solar radio burst peak frequency for nearly all of the events considered, the radio–emitting electrons have energies typically around 100 keV (Nitta & Kosugi 1986; Kosugi, Dennis & Kai 1988). The same result was implied by a comparison of the relative numbers of microwave–emitting and hard–X–ray producing electrons (Kai 1986; Gary 1985).

A very useful property of gyrosynchrotron emission is that the turnover frequency is roughly proportional to the magnetic field strength in the source, and only very weakly dependent on other properties such as density and energy spectrum. The typical turnover frequency of 8 GHz

(Guidice & Castelli 1975; Staehli, Gary & Hurford 1989) corresponds to a magnetic field strength of several hundred Gauss. We note here that in every one of the eight flares we discuss, the peak 15.4 GHz flux in the impulsive phase is $\sim 2 \times$ the 8.8 GHz flux. The "canonical" spectral index of an optically–thick homogeneous nonthermal gyrosynchrotron source is 2.9 (Dulk & Marsh 1982), and if the turnover frequency in such a source were above 15 GHz the 15.4 GHz flux would be $5 \times$ the 8.8 GHz flux, although inhomogeneities in the source tend to produce flatter spectra on the optically–thick side. Thus, we cannot easily determine the turnover frequency from the available data, but it appears to be of order 15 GHz *in each of the flares*. This implies a relatively high magnetic field in the radio sources.

2.4. Soft X–ray data

The Space Environment Monitors aboard the Geostationary Operational Environmental Satellites (GOES) include ion chambers sensitive to X–rays in the wavelength ranges 1 – 8 Å (1.5 – 12.4 keV) and 0.5 – 4 Å (3 – 25 keV). These data are available from the Space Environment Laboratory of NOAA at 3.0 second resolution. It is well established observationally that the soft X–rays (SXR) do not resemble the harder X–rays (> 25 keV) in behaviour, and they are believed to be a signature of hot dense plasma (typical temperature $1 - 2 \times 10^7$ K) in the corona; from the observation that the SXR time profile is often well–matched by the integral of the HXR time profile (Neupert 1968; Dennis & Zarro 1993; it should be noted that Neupert originally used microwave data as a proxy for hard X–ray measurements, which were not available at the time), it is believed that the bulk of the SXR result from material heated by the nonthermal electrons which also produce the HXR.

3. INDIVIDUAL EVENTS

The basic data for each flare are collected in Table 1. The first column gives the flare number which we will use to refer to the events in this paper; this is the same as the relevant figure number. The second column of Table 1 gives the date and approximate start time of the event. The third column gives the flare number in the catalog of BATSE solar flares maintained by the SMM/HXRBS group at Goddard Space Flight Center, while the fifth and sixth columns give the hard X–ray (HXR) duration and the > 25 keV hard X–ray peak count rate (for a collecting area of 2000 cm^2), respectively, from the same catalog. Column 4 is the GOES soft X–ray (SXR) class listed for the event in *Solar Geophysical Data* (SGD); in three cases no class was listed, and we measured the background–subtracted level directly from the GOES data and estimated a class accordingly (these cases are listed in parentheses; note that the classes listed in SGD are not background–subtracted, but since they are all much larger events, subtraction will not significantly change their classes on the logarithmic scale used). Columns 7 and 8 present the peak 8.8 GHz and 15.4 GHz microwave fluxes measured by the RSTN network, in units of sfu; column 9 is the peak correlated millimeter flux in the impulsive phase measured at BIMA at 86 GHz. In two events the peak millimeter flux occurred in the gradual decay phase rather than the impulsive phase, and the corresponding peak fluxes are listed in parentheses. Column 10 is the energy spectral index estimated from the 25–50 keV and 50–100 keV BATSE channels as described above, for a thick target model. One of the features of these flares is that they were all very soft, and the fitting procedure gave photon spectral indices greater than 8 in some cases. Since the spectral response program is not accurate for such soft spectra (R. Schwartz, private communication), we have indicated lower limits in the table in those cases where the

energy spectral index apparently exceeds 9 (photon spectral index exceeds 7.5). Column 11 is the energy spectral index for the radio–emitting electrons calculated using the 15 GHz and 86 GHz fluxes and the assumptions that gyrosynchrotron emission is the radiation mechanism, and that both frequencies are in the optically–thin part of the spectrum. In this case the energy spectral index is approximately $\delta = 1.36 - 1.11\alpha$ (Dulk & Marsh 1982), where α is the radio flux spectral index (negative). In fact it is unlikely that 15 GHz is in the optically–thin part of the spectrum for most of these flares; we discuss the effects of this further below. The final column presents notes relevant to individual events.

3.1. Flare of 20:51 UT, 1991 June 08 (event 416 in the BATSE flare catalog)

This is a very weak flare, but we include it because it demonstrates the sensitivity of both BATSE and BIMA. Figure 1 shows the time profiles of the event in the 86 GHz emission measured by BIMA (solid line), the > 25 keV hard X–rays measured by BATSE (short–dashed line histogram), the 15.4 GHz microwave emission (dotted line) and the GOES 3–25 keV channel (long–dashed line). We have smoothed the BATSE and RSTN data to a time resolution of 4 seconds, the BIMA data to a resolution of 1.6 seconds, and the GOES data to 12 seconds in order to improve the presentation of this figure. The total duration of the event is about 20 seconds in all but the GOES data. We plot all data, including the GOES data, on linear scales for simple comparisons, and all are scaled to the same peak height: the scale for the 15 GHz curve is on the left vertical axis, that for the HXR data is on the right vertical axis, and the scale for the 86 GHz curve can be determined by finding the peak flux in Table 1. The same format will be used in Figures 2 – 8.

This appears to be a very small impulsive event, with the hard X–rays, soft X–rays and millimeter emission all starting at about the same time. No GOES class was recorded for this event, but it was identified as a flare in the BATSE data. The actual enhancement in the GOES 3–25 keV channel was only 1.0×10^{-8} W m^{-2}, while that in the 1.5–12.4 keV channel was $1 - 2 \times 10^{-7}$ W m^{-2} above a background of 2.1×10^{-6} W m^{-2}. Thus, this event would be classified as a B1 flare from its GOES data, which is a very small event indeed. Nonetheless, it shows impulsive emission at 86 GHz, indicating production of MeV–energy electrons, as well as in hard X–rays below 100 keV. A peak of approximately 10 sfu is seen in the 15 GHz data, but occurring slightly (10 s) later than the peaks in HXR and millimeter. There was no detectable microwave emission at lower frequencies (8.8 GHz flux < 5 sfu). The energy spectral index calculated from the X–ray data is unreliable due to the low count rate in the 50 – 100 keV channel.

Millimeter emission was only reliably detected on baseline 31 (i.e., the baseline between antennas 3 and 1, with a fringe spacing of $\sim 20''$ east–west at the time of the burst). The closure phase for this event is not consistent with zero. However, we suspect that this is due to the correlated amplitude being dominated by large–scale structures in the active region, which is consistent with seeing the greatest contrast on the baseline sensitive to the smallest features. The vector subtraction of the preflare emission which is carried out on all data in determining closure phase will not be effective if the background level is varying rapidly on a short timescale. Consequently, we have no convincing evidence on the size of this flare at 86 GHz.

3.2. Flare of 19:56 UT, 1991 June 10 (event 471)

The data for this flare are presented (at full resolution) in Figure 2, using the same format as in Fig. 1. Based on the background–subtracted GOES flux this was a C1.5 enhancement over the background level. The HXR show a very sharp onset and a simple profile with emission lasting

only about 20 seconds. The 15.4 and 86 GHz profiles both peak 5 s after the HXR peak. The 15 GHz profile starts rising slowly at about the time of HXR onset, while the 86 GHz profile starts to rise about 10 seconds after HXR onset but then rises more sharply than the 15 GHz data. Both 15.4 and 86 GHz data show a fairly sharp rise and an approximately exponential delay, with the 15.4 GHz data having a longer decay time; they also show a slightly more rounded peak than do the 86 GHz data. The SXR start to rise before the onset in HXR.

In this event the 86 GHz fluxes were similar on all three baselines, and the closure phase is consistent with zero, implying that the 86 GHz source was probably smaller than about one–third of the shortest fringe spacing, or 6″.

3.3. Flare of 17:25 UT, 1991 June 11 (event 497)

The data for this flare are presented in Figure 3. The 86 GHz data have been smoothed to about 25 seconds resolution in time to improve the clarity of the figure: there are no significant structures in the 86 GHz data with timescales smaller than this, but the point–to–point variability was quite high (we discuss this fact further below). The HXR data for this GOES–class M1 flare show two simple peaks of about equal strength, 7 minutes apart. This flare occurred just after GRO emerged from the Earth's shadow into sunlight, and it is possible that some of the emission in the rise was missed, but from the relation of the HXR to the microwave peak we believe that GRO did catch the HXR peak. The SXR data rise quickly in conjunction with the first HXR peak, and then show only a small additional enhancement associated with the second HXR peak. The second peak is actually harder in spectrum than the first. The 15.4 GHz data show an impulsive peak exactly coincident with the first HXR peak to within the time resolution of the data (1.0 s), and very little emission associated with the second HXR peak: interestingly, the second impulsive peak appears to contribute more flux at 8.8 GHz than at 15.4 GHz even though all the other events discussed here have a higher 15.4 GHz flux. The 86 GHz data, on the other hand, show no enhancements associated with either HXR peak (< 0.1 sfu). Rather, they show a very slow evolution similar to a gradual–rise–and–fall event (GRF). The 86 GHz data peak later than the SXR fluxes do, but this is somewhat illusory since the radio flux produced by the SXR–emitting material rises as the material cools, and is not expected to peak until after the SXR peak. We discuss this further below. The BIMA flux is only of order 1 sfu at its peak, whereas the flux expected from the GOES material is of order 10 sfu, but the fluxes on the different 86 GHz baselines are quite different, and the closure phase is not consistent with an unresolved source, so we are confident that the true millimeter source size is too large to be measured by BIMA (> 20″). This appears to be a moderate–sized event in which HXR and microwave–emitting electrons were produced, but insufficient millimeter–emitting MeV–energy electrons were accelerated in the impulsive phase to produce an 86 GHz signature. Rather, the millimeter emission is a signature of the dense plasma in the corona after the impulsive phase.

3.4. Flare of 01:33 UT, 1991 June 12 (event 502)

By contrast, this event was small in the impulsive phase at all wavelengths except millimeter. From the data in Figure 4 it may be seen that the SXR rise even in the 3–25 keV channel is barely evident; in the 1.5–12.5 keV channel it is at most 1×10^{-7} W m^{-2}, corresponding to B1 level. The HXR data show a single spike of duration < 15 seconds (the HXR data have been smoothed to 4 s resolution to improve the appearance of the figure), while the millimeter data show a spike (4 sfu) with a sharp rise and nearly exponential decay, peaking 2 s after the HXR peak. The 86 GHz data show no significant thermal phase after this spike, consistent with the

small soft X–ray signature. The 15 GHz data show a small spike of about 20 sfu coincident with the millimeter spike. Compared with the previous event, the soft X–ray production was more than two orders of magnitude smaller in this event and the 15 GHz flux and HXR peaks were smaller by a factor of 4, but the 86 GHz flux associated with the impulsive phase was at least 30 times larger. The flux and time profile of the 86 GHz emission were the same on all three baselines and the closure phase is consistent with zero, so the 86 GHz source was compact ($< 6''$).

3.5. Flare of 16:03 UT, 1991 June 12 (event 507)

The data for this event are shown in Figure 5. In this case both the HXR and 86 GHz data show strong emission continuing for approximately 1 minute, with both a sharp onset and a sharp switch–off. However, the two HXR sub–peaks do not coincide with the 86 GHz peak. The 15 GHz data show an altogether smoother profile, with a more gradual rise, a simple peak and a decline much more gradual than in HXR and at 86 GHz. The SXR data do not start to rise until the impulsive phase in HXR begins. The longer baselines show an extended thermal phase at 86 GHz, peaking later than the GOES flux has peaked and lasting for over 10 minutes. Thus this event is marked by the differences between the 15 GHz and 86 GHz profiles.

In the impulsive phase the 86 GHz emission has a similar time profile on all baselines but appears to be strongest on the shortest baseline. The closure phase is consistent with zero throughout the impulsive phase at 86 GHz, and phases on the individual baselines show no rapid changes which might indicate contributions from separate sources more than $10''$ apart. We therefore believe that the 86 GHz source was a simple source of dimension $10''$ – $20''$ and therefore slightly resolved on our baselines (which were $\sim 49''$, $97''$ and $32''$ at the time of the burst).

3.6. Flare of 17:07 UT, 1991 June 12 (event 508)

In this event the data all have fairly simple time profiles (Figure 6). The HXR data show two peaks 10 seconds apart and emission lasting for $\sim$ 1 minute; however the HXR data are difficult to interpret due to a rapidly changing background level which we assume is non–solar, and for this reason the spectral index based on the HXR data is highly uncertain. The 15 GHz data start to rise 40 seconds before they (and the HXR) peak, while the 86 GHz data start to rise 30 seconds later and peak much more quickly. The 86 GHz data show only a single peak, nearly coincident with the second HXR peak, and delayed by 8 seconds with respect to the first HXR peak. The 15 GHz data peak at about the same time as the 86 GHz peak and the second HXR peak, but again show a time profile with a more rounded peak and a much slower decay than at 86 GHz.

The 86 GHz data again show a pronounced gradual phase on the shorter baselines, lasting for approximately 15 minutes after the impulsive phase. In the impulsive phase the three baselines again have similar time profiles but the fluxes are largest on the shortest baselines (which also see the largest post–flare fluxes). The closure phase is again consistent with zero during the impulsive phase, but not during the decay phase. Therefore the spatial properties of this source are similar to that of the preceding flare.

3.7. Flare of 20:08 UT, 1991 June 13 (event 524)

This is another event in which the 86 GHz data show very little impulsive–phase emission. In Figure 7 a small enhancement at 86 GHz may be seen coincident with the impulsive spikes seen in HXR and at 15 GHz; both these wavelengths show a second, much less impulsive emission 2 minutes later. However, the 86 GHz data peak coincident with the GOES data in

this event, and are thus presumably dominated by free–free emission from hot dense plasma in the post–flare phase. The largest 86 GHz flux is measured on the shortest baseline, and the time profile on the other baselines is quite different. The closure phase is not consistent with zero at any stage. Note that the point–to–point variation in the 86 GHz data is high: it is much higher than the preflare noise level, as was the case in Fig. 3. The impulsive 15 GHz peak again shows a slower decay than does the HXR emission.

3.8. Flare of 01:27 UT, 1991 June 14 (event 527)

The last flare we discuss is the largest in this paper, a GOES class M7 event. Unfortunately, the initial part of this flare occurred while the Earth was still occulting *Compton/GRO* from the Sun, but the spacecraft passed out of the Earth's shadow at 01:29:50 and there was no enhancement in the HXR level at this time. One minute later, BATSE detected the onset of HXR emission which was to last for 10 minutes, with 4 main peaks in HXR. The 86 GHz and microwave data show their strongest emission during an impulsive peak at 01:27, while BATSE was occulted, and it might be thought that the HXR also peaked at that time. However, the GOES data show only a very small rise associated with the event at 01:27, while the rise starting at 01:31 and continuing until 01:40 is at least an order of magnitude larger. Based on the usual correlation between HXR and SXR, we therefore conclude that the HXR emission at 01:27 was probably weaker than in the peaks starting at 01:31. The peak HXR rate was no greater than in several other events described above, but the HXR emission lasted for much longer than in any of the other events and this is consistent with the large GOES class. The 86 GHz data also show non–impulsive emission continuing through the thermal decay phase of the flare.

The Sun was close to setting at the time of this event, so the BIMA fringe spacings are all large (70″, 140″ and 45″). As in the other events with impulsive–phase emission at 86 GHz, the peak flux was similar on all baselines and the closure phase consistent with zero, implying a source of dimension $< 10''$.

4. GENERAL RESULTS

This study has several aims. The first is to establish the properties of millimeter emission for a wide range of flare sizes, and particularly their correlation with properties in other wavelength ranges. The second is to use these comparisons to investigate the behaviour of electrons in different energy ranges. As a prelude to the second discussion, here we review the results of comparing data in different wavelength ranges.

4.1. Energetic electron production versus flare size

The study here confirms the result of previous studies (Kundu et al. 1990; White et al. 1992; Lim et al. 1992) on the production of energetic electrons capable of radiating at millimeter wavelengths: this can take place in the smallest flares detectable, as well as in the largest. Assuming that the millimeter emission is due to MeV–energy electrons radiating by the gyrosynchrotron mechanism, we interpret this as evidence that there is no "threshold" effect in the acceleration of electrons to MeV energies, i.e., there is no minimum flare size above which such acceleration takes place. If the mechanism for accelerating electrons to MeV energies is related to that for accelerating ions, then equally we expect no threshold effect in the production of energetic ions; however, presently we have no detection method for such ions comparable in sensitivity to millimeter interferometry.

The only plausible alternative interpretation of the impulsive millimeter emission is free–free emission by material much cooler than the GOES–emitting material: however, the small source sizes measured here together with the large fluxes imply brightness temperatures in excess of 2 $\times$ 10^5 K, and if this is thermal material, then the radio flux from it should rise as it cools; we therefore believe that the rapid decay of the impulsive 86 GHz emission on timescales comparable to that of the HXR emission is not consistent with cooling thermal material.

4.2. Relation of HXR rates and millimeter fluxes

Another important result of this study is that there is no simple relation between the production of HXR and microwave–emitting electrons and the production of millimeter–emitting electrons in the impulsive phase. In some events (3, 7, 8) the HXR and microwave fluxes are high while there is negligible 86 GHz emission associated with them; in others (4), the millimeter emission seems surprisingly strong given the weak level of HXR and microwaves. There are, however, many other parameters which will affect the relative production of HXR, microwaves and millimeter emission from a given electron distribution. The most important is probably magnetic field strength, since the millimeter emission is a very sensitive function of this. However, to the extent that the microwave spectrum can be used to estimate the magnetic field, it seems to have been similar in all eight microwave sources since they all have nearly the same (high) turnover frequency. Thus this cannot explain the high variability in the ratio of millimeter emission to other properties. Further, Kosugi *et al.* (1988, see also Kai *et al.* 1985) find that for large flares the ratio of peak 17 GHz flux to peak > 30 keV HXR flux (which should also depend strongly on magnetic field) has a scatter of only a factor of about 2.5 over several orders of magnitude in flare size, whereas just in these eight flares the ratio of 86 GHz flux to peak HXR flux in the impulsive phase varies by at least a factor of 400. By contrast, the ratio of the 15.4 GHz flux to the peak HXR count rate in these events varies by only a factor of 3. We also note that none of the millimeter sources detected in the impulsive phase showed any evidence that they were large and that therefore BIMA was not seeing most of the flux (in contrast to the decay phase), so the spread cannot be explained by this effect. An acceleration mechanism for the MeV–energy electrons which is to some extent independent of the production of the lower–energy electrons producing the HXR emission is consistent with these data.

4.3. Onset of millimeter and microwave emission

Lim *et al.* (1992) noted that the onset of microwave emission at 15 GHz usually precedes the onset of impulsive emission at millimeter wavelengths, and this result is also found here, in every event with sufficient signal–to–noise. Thus, the lower–energy microwave–emitting electrons seem to be produced earlier. The difference occurs because the microwave emission tends to turn on relatively gradually, whereas the millimeter emission tends to turn on very sharply. The simple spike profile of the impulsive 86 GHz emission seen in events 2, 4, 6, and 8 occurs commonly: we discuss this further elsewhere (**?**).

4.4. Delays between high–energy and low–energy electrons

In Figure 2 both the HXR and the millimeter emission have a sharp onset, and there is an unambiguous delay, of order 10 seconds in this case, of the millimeter emission with respect to the HXR emission. In several other events there is evidence for delays in the same sense, although smaller; in no event (including others not presented here) have we seen the millimeter onset lead the HXR onset. Since we argued at the outset that both the HXR and microwaves

are associated with electrons of energy lower than those which produce the millimeter emission, this result and the previous one are consistent with a delay in the production of the MeV–energy electrons.

The measurement of delays between the time of production of high-energy electrons and of low-energy electrons is an important observational constraint to theories for energetic particle production in solar flares. It clearly has a bearing on whether all energetic particles in the impulsive phase are accelerated by the same mechanism, or whether one mechanism is required for the lower–energy electrons carrying the bulk of the energy, and another for the higher–energy electrons. In fact, the delay in Fig. 2 is so large (about 10 seconds) that it may be too large to be attributed to an acceleration time in a continuous acceleration mechanism, and may instead reflect a "switch–on" time.

Most studies of delays until now have been restricted to the very large events in which sufficient counts in higher energy channels are recorded by the hard X–ray instruments. However, large flares are usually notoriously complex, and the measurement of delays for complex events is very difficult. Millimeter observations offer the chance to study the energetic component in smaller, simpler flares.

4.5. Energy spectra

We noted above one peculiarity shared by most of the smaller flares from AR 6659: they all have an unusually high turnover frequency. A second peculiarity may be seen in Table 1: the impulsive HXR emission appears to be particularly soft in all cases. As we noted above, in many cases the spectra were too soft to be fit reliably with a power law index from the two–channel data. As a check that these flares were genuinely softer than "typical" flares, we arbitrarily selected a sample of flares from the BATSE database and compared the ratio of the counts in the 25–50 keV and 50–100 keV channels. The selection criterion used was a peak count rate between 10000 and 11000 in the BATSE catalog, which should pick up moderate sized flares with no strong bias towards any one type of flare. The resulting list contained 26 flares, of which 1 appeared to be a non–solar burst and 1 other was omitted from consideration because only the decay phase was observed. Two of the flares were from AR 6659, the same region which produced the flares discussed here, including event 7. For the remaining 22 flares the ratio of the peak rate in channel 1 to that in channel 2 (both background–subtracted) had a mean of about 4.5. The largest ratio of all the flares (> 20) selected in this way belonged to event 528 in the BATSE catalog, which came from AR 6659 on June 14. For the 8 flares from AR 6659 discussed here the corresponding mean was 10.9, with individual events ranging from 7 to ~ 100. Thus it is clear that these events were truly softer than average. One possible reason for this would be a "superhot" thermal component (Lin et al. 1981) present in the 25–50 keV channel for the flares from this region, particularly if the lower edge of this channel, which is not well determined at present, extends down below 25 keV.

Even though the energy spectral index deduced from the ratio of the 15 GHz flux to the 86 GHz flux is uncertain since the turnover frequency seems to be of order 15 GHz, the difference between the spectral indices deduced from the HXR and millimeter observations is very large in all cases and they probably cannot be reconciled. It appears difficult to escape the conclusion that there is a flat component to the energy distribution at high energies which is not reflected in the < 100 keV HXR. Vestrand (1988) has discussed evidence for a similar effect in SMM/GRS data. We will carry out a more detailed study of this question for two other events in this period for which better X–ray spectra exist (**?**); here we note one important implication. Since

the excellent correlation between flare microwave emission and HXR emission was first noticed (Kundu 1961) and they were attributed to the same electron population, it has been realized that the HXR appear to require many more electrons than does the microwave emission. This was partly solved when it was realized that the thin target assumption for production of the HXR, which had been used in most early calculations, requires many more electrons than does the thick–target assumtion which is now more prevalent, and that with the thick–target assumption there does not seem to be a severe number problem (e.g., see the recent discussions of this issue given by Gary 1985 and Kai 1986). However, in these discussions of this issue the electron energy distribution implied by the microwave data has not been determined through the lack of suitable high–frequency observations, and it is always assumed that the energy distribution derived from the HXR data is the one which applies. As soon as one accepts the possibility that the spectrum of the radio–emitting electrons is flatter than the spectrum of the HXR–emitting electrons, the problem disappears.

4.6. Thermal bremsstrahlung at millimeter wavelengths

It is well established that the decay phase of flares usually involves a large amount of hot, dense, soft–X–ray–emitting plasma, and it is easily shown that this plasma will produce a significant radio flux. Since at high frequencies this flux is effectively independent of frequency, its contribution relative to any nonthermal emission, which has a flux spectrum falling with frequency, will increase. Several of the events described here show a smooth, post–impulsive–phase emission at 86 GHz which clearly resembles the expected signature of free–free emission from post–flare loops, although only in Figures 3, 7 and 8 do we show a long enough time period for this to be evident. In many events both an impulsive phase and a gradual thermal phase are seen at 86 GHz. The GOES fluxes can be used to calculate a temperature and emission measure for this material (Thomas, Starr & Crannell 1985), and thus the expected 86 GHz flux may be derived (White & Kundu 1992; note that the expression given there is for one polarization only, and should be multiplied by 2 for comparison with RSTN data). It amounts to less than 10 sfu in every event except 8, where the predicted flux is almost 50 sfu at 01:45 UT. In both events 3 and 8, the predicted flux is strong enough to be compared with the microwave data, and is found to be close to the measured 15.4 and 8.8 GHz fluxes in the late decay phase. In Figure 9, we compare the radio flux predicted from the GOES data with the 15.4 and 8.8 GHz fluxes for event 3; the estimated temperature of the GOES material is also shown. The predicted radio flux can be seen to peak after the SXR 3 – 25 keV flux peaks (see Fig. 3), although its peak is coincident with the peak in the 1.5 – 12 keV SXR channel. As is usual, the soft–X–ray–emitting material is hottest in the impulsive phase and cools thereafter; as it cools, the radio flux rises. It may be seen that the microwave fluxes are very close to the prediction of free–free theory in the late decay stages of this event (after about 17:40 UT). As noted earlier, the observed correlated 86 GHz flux is much smaller than predicted, and this is true of all the events here in which a comparison can be made. This is in fact expected: the post–flare loops are known to cover a large area, but the interferometer is insensitive to large sources and is not expected to measure all the flux present. The microwave data, which measure the full–disk flux, do not suffer this effect.

An alternative explanation of the post–impulsive–phase emission would be nonthermal radiation due to some second–stage aceleration of electrons, e.g. in a coronal shock, which might not produce much HXR emission but could still produce radio emission. Although we cannot rule this out, we feel that the thermal bremsstrahlung explanation is to be preferred. The

strongest argument is that even if there were some contribution from a nonthermal component, we should still see thermal bremsstrahlung from the known SXR–emitting material present, and the calculations show that the expected flux is generally larger than we observe, while the timescales of the post–impulsive–phase millimeter emission match the SXR timescales. Thus presently we have no evidence for a component in the decay phase which cannot be explained by thermal bremsstrahlung.

A common feature of these post–impulsive–phase emissions at 86 GHz (as seen by the interferometer) is that they show a large point–to–point variability, such as is seen in Figure 7. This "noise" level is much higher than the intrinsic noise level in the data, as seen for example in the data prior to the flare. We believe that the reason for this lies in the fact that the total flux from the field of view is much larger than the interferometer can measure, since it is distributed on large spatial scales. Then relatively small changes in the shape of the source, or its brightness at different locations, will still have an effect on the interferometer amplitude: these changes amount to a small fraction of the total flux, but can be a large fraction of the correlated amplitude, and thus can appear as an elevated "noise" level.

5. CONCLUSIONS

We have carried out the first extensive comparison of observations of solar flares at millimeter wavelengths with hard X–ray data, covering a wide range of flare sizes. Based on both theory and observation, the millimeter emission of flares in the impulsive phase should be a diagnostic of the most energetic electrons accelerated in these flares. Typically we expect the millimeter emission to arise from electrons with energies in excess of 1 MeV; it is unlikely that electrons with energies below 0.5 MeV contribute any significant millimeter emission.

We find that such energetic electrons are produced in flares of all sizes, including flares so small that their soft X–ray signature is barely detectable. Further, their behaviour is not consistent with their energy distribution being a simple extension of the distribution of the electrons with energies below 200 keV which produce the observed HXR below 100 keV. We emphasize that there are many effects which influence the relative levels of HXR and radio emission by energetic electrons, and their time profiles. In particular, since we assume that the radio emission is produced by electrons in the corona while the HXR emission is produced by electrons striking the chromosphere, trapping of electrons in the corona plays a major role in determining both the relative peak fluxes, and the relative time behaviour. For this reason the time profile of the 86 GHz emission cannot simply be interpreted as the rate of acceleration of MeV–energy electrons. A number of the effects which can arise have been explored by Petrosian and co–workers (Petrosian 1982; Lu & Petrosian 1989; Lu & Petrosian 1990). We will consider this issue in more detail elsewhere (**?**). However, all the available evidence seems to suggest that the millimeter–emitting electrons form a different population from the HXR–emitting electrons: the lack of close correlation with the HXR profile, the lack of agreement between the energy spectral indices derived from the radio and HXR data, the time delay in the onset of the millimeter emission (a delay of the peak is readily explained in a trap model, but a delay in the onset cannot be so readily explained in this way), and the wide range of variability found in the ratio of peak millimeter flux to peak HXR count rate from flare to flare. If they are indeed a different electron population this has obvious implications for the acceleration of electrons in solar flares: it may imply that separate acceleration mechanisms are required for electrons at high and low energy ranges. We plan to explore this issue further elsewhere.

Acknowledgements

The ready availability of GRO/BATSE solar flare data and GOES soft X–ray data at the Goddard Space Flight Center's Solar Data Analysis Center has been crucial for making it easy to compare data over different wavelength ranges, and we gratefully acknowledge the assistance of Richard Schwartz, Kim Tolbert and Gordon Labow in this regard. In addition, we have made use of the BATSE detector response program written by Richard Schwartz and we thank him for allowing us to use it. The referee, Brian Dennis, is thanked for his careful reading of the paper and his thoughtful comments and suggestions. Markus Aschwanden is acknowledged for a number of helpful discussions, and for assistance with access to some of the Goddard programs. The RSTN microwave data were obtained with the assistance of Greg Deuel. We also acknowledge the hard work Alan Kiplinger and Dave Speich devoted to maintaining communications within the community of solar observers during the campaign–of–opportunity which took place during 1991 June, and from which this research benefited.

This work was supported by NASA's GRO Phase I Guest Investigator program under grant NAG–5–1540. Partial support was also received from NASA grant NAG–W–1541 and NSF grant ATM 90–19893. The use of BIMA for scientific research at the University of Maryland is supported by NSF grant AST 91–00306.

Bibliography

Brown, J. C. 1971, *Solar Phys.*, 18, 489.

Dennis, B. R., & Zarro, D. M. 1993, *Solar Phys.*, 146, 177.

Dulk, G. A., & Marsh, K. A. 1982, *Astrophys. J.*, 259, 350.

Gary, D. E. 1985, *Astrophys. J.*, 297, 799.

Guidice, D. A., & Castelli, J. P. 1975, *Solar Phys.*, 44, 155.

Holt, S. S., & Ramaty, R. 1969, *Solar Phys.*, 8, 119.

Kai, K. 1986, *Solar Phys.*, 104, 235.

Kaufmann, P., Correia, E., Costa, J. E. R., Vaz, A. M. Z., & Dennis, B. R. 1985, *Nature*, 313, 380.

Kosugi, T., Dennis, B. R., & Kai, K. 1988, *Astrophys. J.*, 324, 1118.

Kundu, M. R. 1961, *J. Geophys. Res.*, 66, 4308.

Kundu, M. R., White, S. M., Gopalswamy, N., Bieging, J. H., & Hurford, G. J. 1990, *Astrophys. J. (Lett.)*, 358, L69.

Lim, J., White, S. M., Kundu, M. R., & Gary, D. E. 1992, *Solar Phys.*, 140, 343.

Lin, R. P., Schwartz, R. A., Pelling, R. M., & Hurley, K. C. 1981, *Astrophys. J. (Lett.)*, 251, L109.

Lu, E. T., & Petrosian, V. 1989, *Astrophys. J.*, 338, 1122.

Lu, E. T., & Petrosian, V. 1990, *Astrophys. J.*, 354, 735.

Neupert, W. M. 1968, *Astrophys. J. (Lett.)*, 153, L59.

Nitta, N., & Kosugi, T. 1986, *Solar Phys.*, 105, 73.

Petrosian, V. 1982, *Astrophys. J. (Lett.)*, 255, L85.

Ramaty, R. 1969, *Astrophys. J.*, 158, 753.

Staehli, M., Gary, D. E., & Hurford, G. J. 1989, *Solar Phys.*, 120, 351.

Takakura, T. 1967, *Solar Phys.*, 1, 304.

Takakura, T. 1972, *Solar Phys.*, 26, 151.

Thomas, R. J., Starr, R., & Crannell, C.-J. 1985, *Solar Phys.*, 95, 323.

Vestrand, W. T. 1988, *Solar Phys.*, 118, 95.

White, S. M., & Kundu, M. R. 1992, *Solar Phys.*, 141, 347.

White, S. M., Kundu, M. R., Bastian, T. S., Gary, D. E., Hurford, G. J., Kucera, T., & Bieging, J. H. 1992, *Astrophys. J.*, 384, 656.

Table 1. Flares in this study

	Time (UT)	BATSE flare num.	GOES SXR class	HXR dur. (sec.)	Peak HXR rate >25 keV	8.8 GHz flux (sfu)	15.0 GHz flux (sfu)	86 GHz flux (sfu)	Energy spec. index (HXR)	Energy spec. index (radio)	Notes
1.	**08 June 20:51**	416	(B1)	28	474	< 5	12	0.3	(7)	3.7	HXR spectral index uncertain due to low count rate.
2.	**10 June 19:56**	471	(C1.5)	48	2669	45	75	1.0	8	4.1	10 second delay of 86 GHz with respect to HXR.
3.	**11 June 17:25**	497	M1.1	208	6560	35	95	< 0.1 (0.7)	> 9 8	> 5.7	Upper limit to impulsive flux at 86 GHz; GRF only. Two HXR peaks, with the first softer than the second.
4.	**12 June 01:33**	502	(B1)	16	1112	< 5	20	4.0	8	2.4	
5.	**12 June 16:02**	507	C4.0	142	4526	50	110	4.0	> 9	3.5	
6.	**12 June 17:06**	508	C7.7	80	13534	90	180	5.2	(8)	3.6	HXR spectral index uncertain due to highly variable background.
7.	**13 June 20:08**	524	C4.4	182	10594	45	100	0.1 (0.7)	8 > 9	5.8	GRF peak stronger than impulsive peak at 86 GHz. Two HXR peaks, with the first harder in spectrum
8.	**14 June 01:27**	527	M7.3	1070	11864	90	170	18.0	> 9	2.8	Four HXR peaks, all with very soft spectra. Main impulsive phase seen in radio occurred during BATSE night

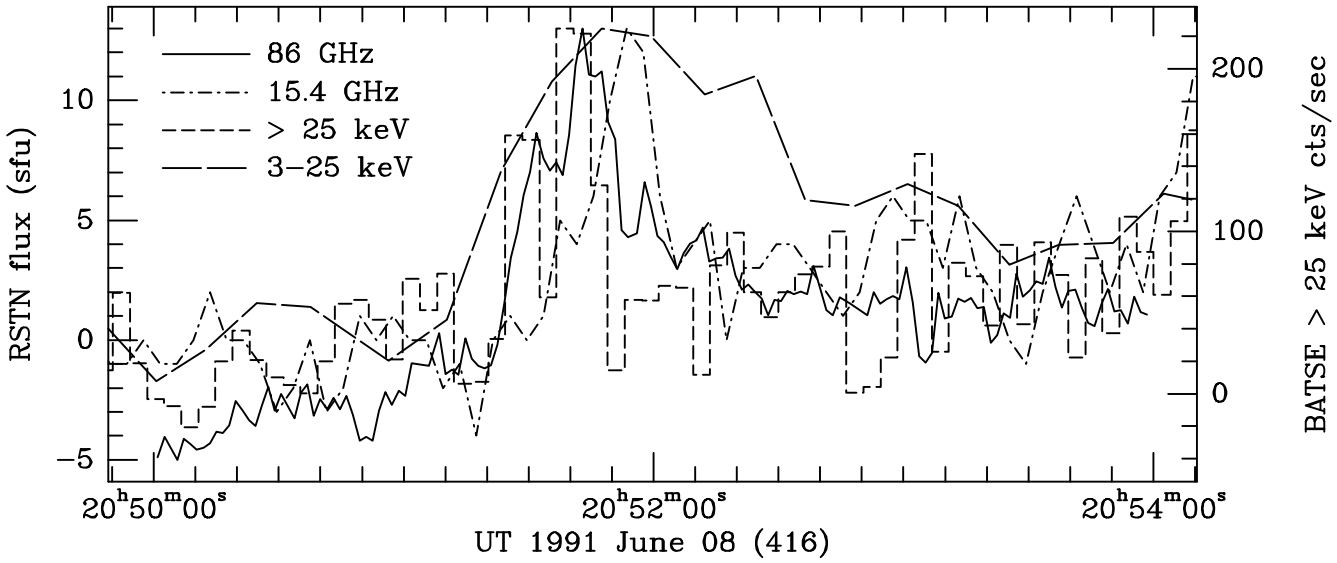

Figure 1. The millimeter (86 GHz from BIMA, solid line), microwave (15.4 GHz from RSTN, dash–dotted line), hard X-ray (> 25 keV count rate from BATSE, dashed histogram) and soft X–ray (3 – 25 keV from GOES, long dashed line) data for the flare at 20:52 UT on 1991 June 8. This flare was very weak, and to improve the presentation of the data they have all been convolved to reduced time resolution (see text). The left axis gives the scale for the 15.4 GHz curve, and the right axis gives the scale for the hard X–ray emission. All curves have been scaled to the same peak height on the figure; the scale for the BIMA data can be determined from the peak flux reported in Table 1. The same format is used in Figures 2 – 8.

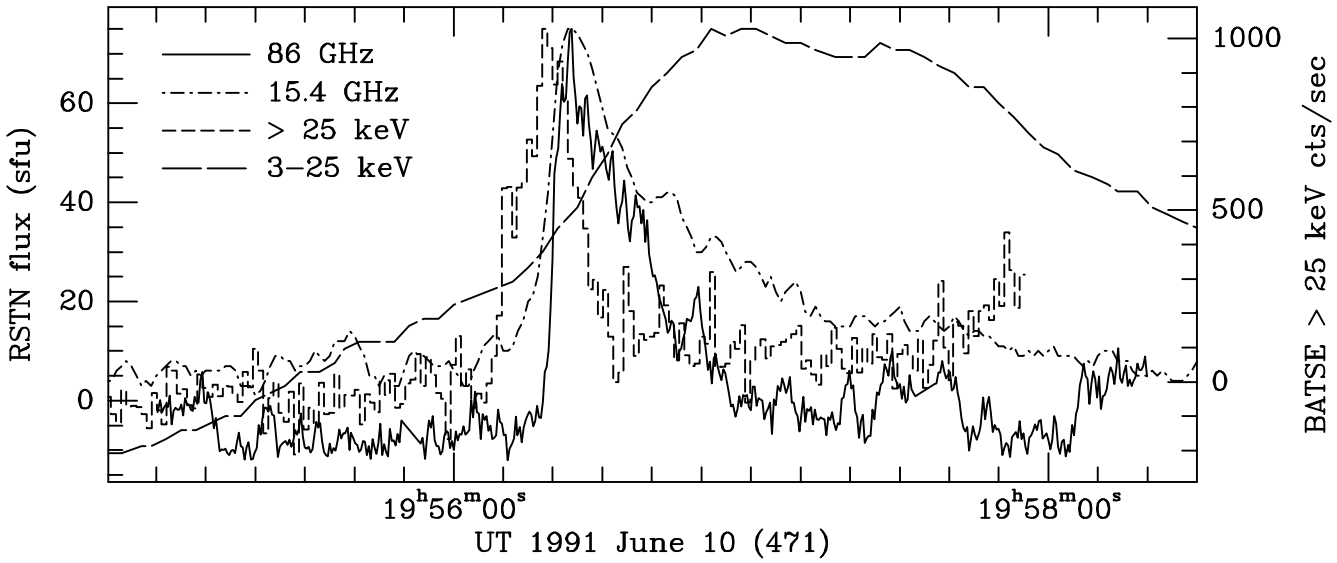

Figure 2. The millimeter (86 GHz, solid line), microwave (15.4 GHz, dash–dotted line), hard X-ray (> 25 keV count rate, dashed histogram) and soft X–ray (3 – 25 keV, long dashed line) data for the flare at 19:56 UT on 1991 June 10.

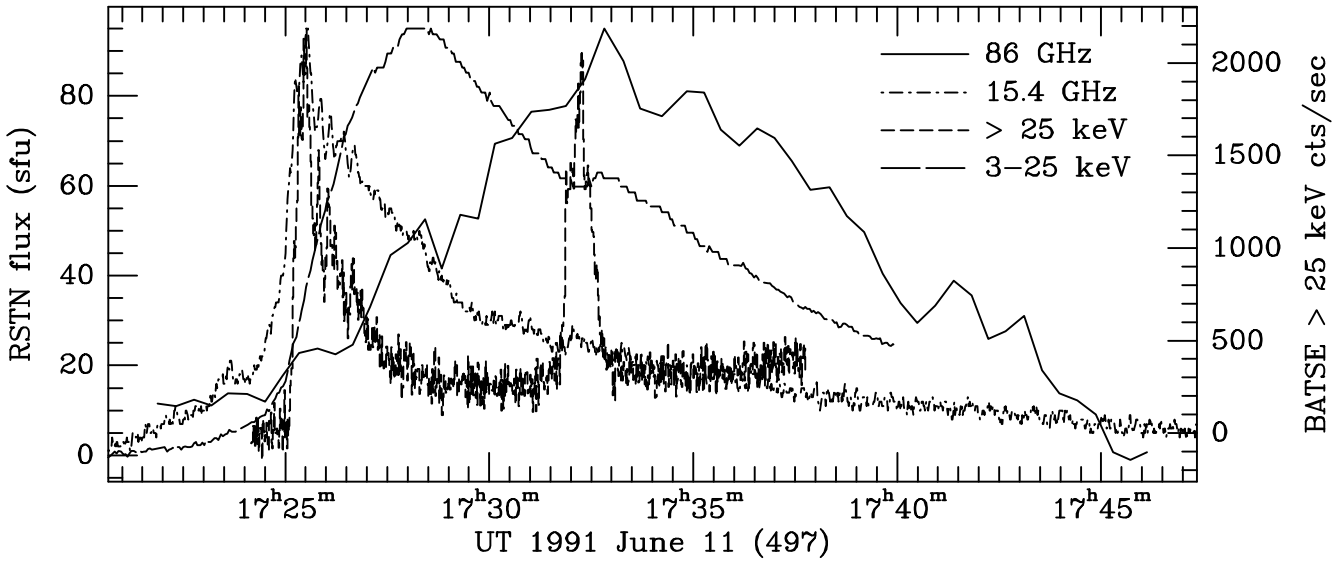

Figure 3. The millimeter (86 GHz, solid line), microwave (15.4 GHz, dash–dotted line), hard X-ray (> 25 keV count rate, dashed histogram) and soft X–ray (3 – 25 keV, long dashed line) data for the flare at 17:25 UT on 1991 June 11. The millimeter data have been convolved to a resolution of 25 seconds to improve the clarity of the figure: they show a high peak–to–peak dispersion at full 0.4 second resolution, similar to that seen in Figure 7. GRO emerged from spacecraft night at 17:25 UT and some of the rise phase of the HXR emission may have been missed.

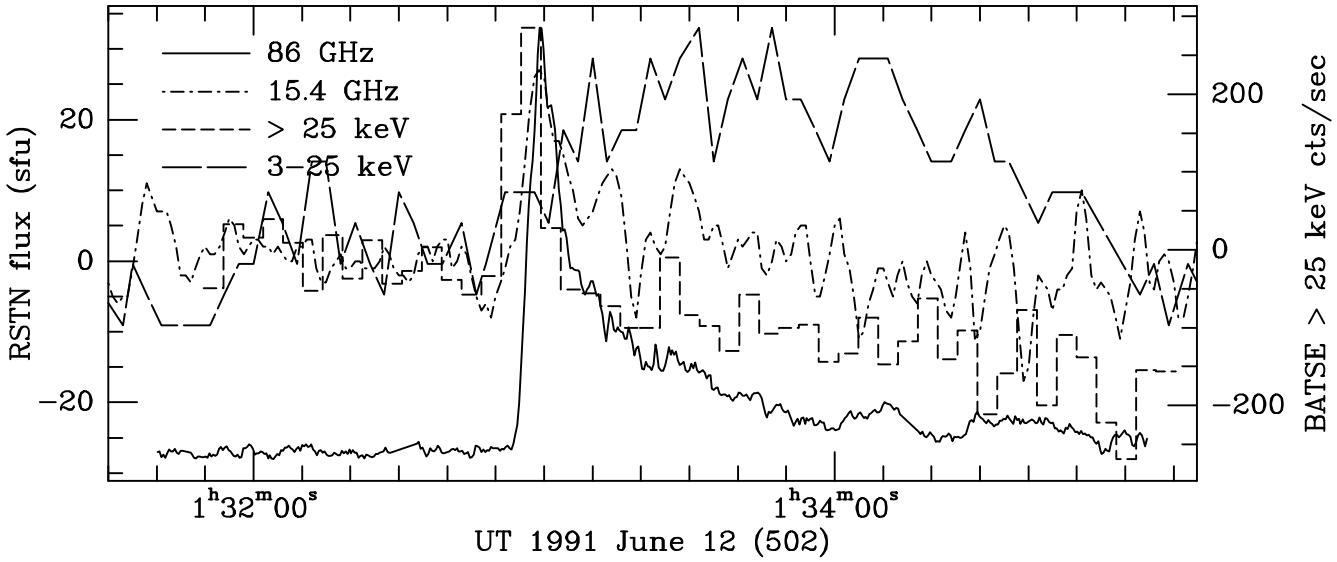

Figure 4. The millimeter (86 GHz, solid line), microwave (15.4 GHz, dash–dotted line), hard X-ray (> 25 keV count rate, dashed histogram) and soft X–ray (3 – 25 keV, long dashed line) data for the flare at 01:33 UT on 1991 June 12. The hard X–ray data have been smoothed to 4.1 s time resolution to improve the appearance of the figure.

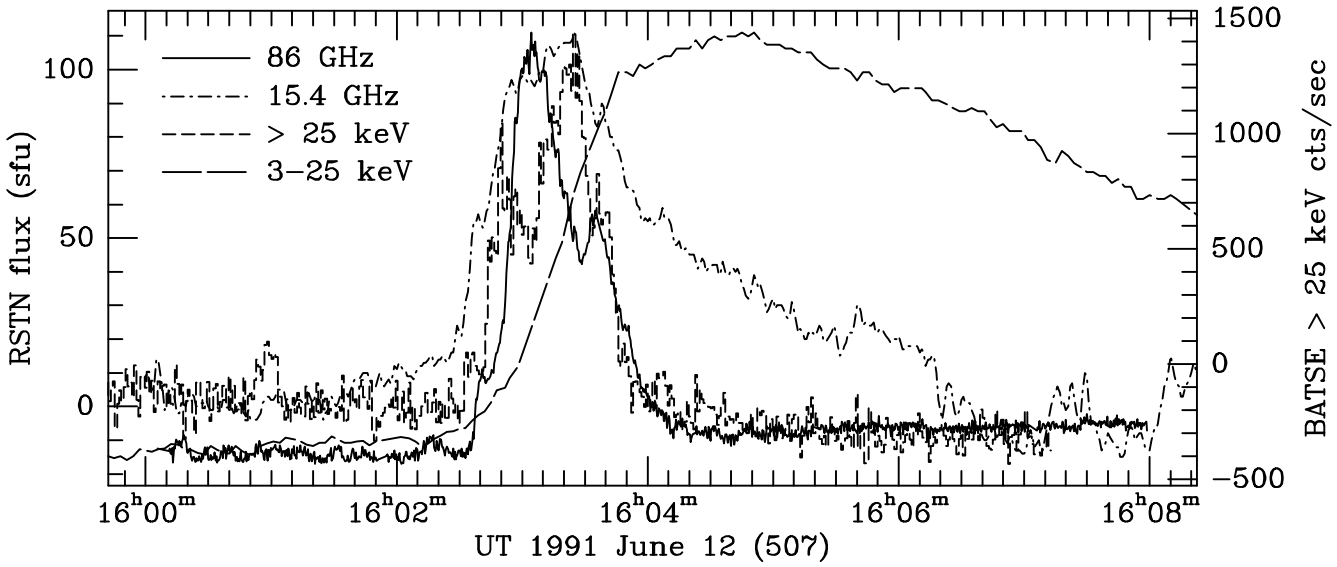

Figure 5. The millimeter (86 GHz, solid line), microwave (15.4 GHz, dash–dotted line), hard X-ray (> 25 keV count rate, dashed histogram) and soft X–ray (3 – 25 keV, long dashed line) data for the flare at 16:03 UT on 1991 June 12.

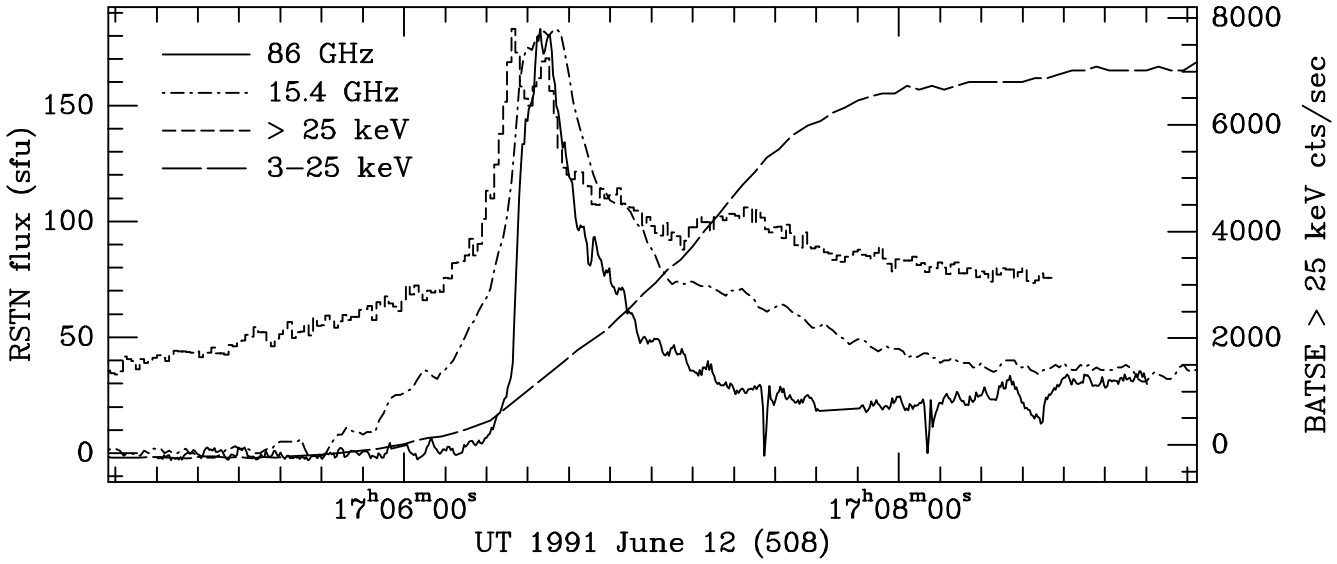

Figure 6. The millimeter (86 GHz, solid line), microwave (15.4 GHz, dash–dotted line), hard X-ray (> 25 keV count rate, dashed histogram) and soft X–ray (3 – 25 keV, long dashed line) data for the flare at 17:07 UT on 1991 June 12.

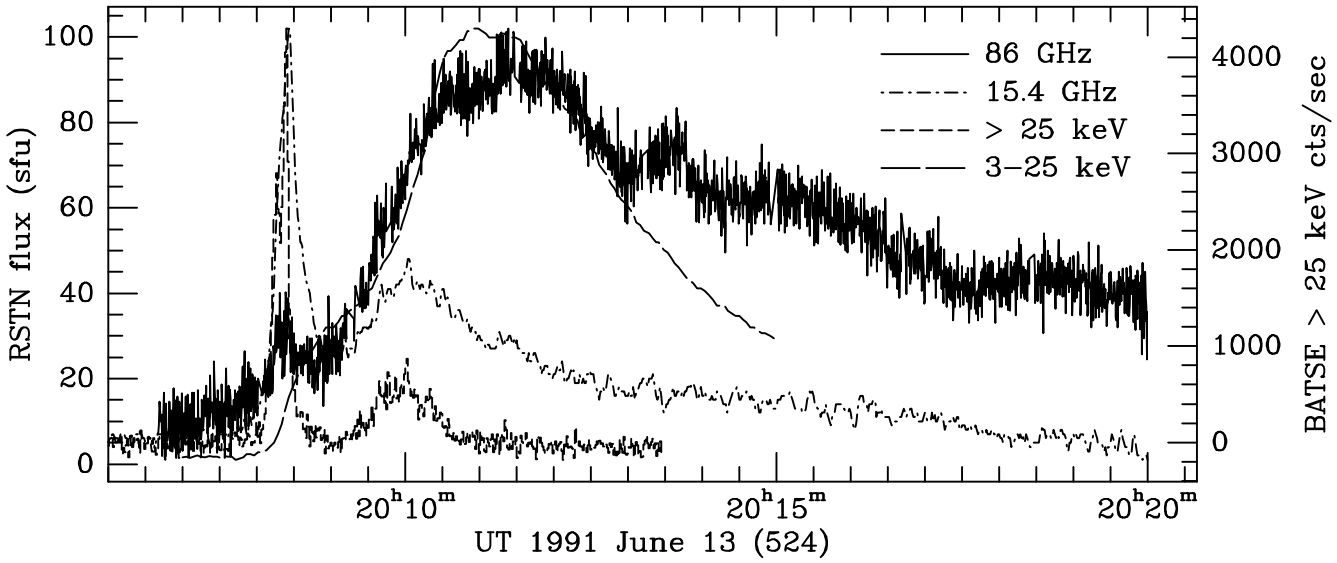

Figure 7. The millimeter (86 GHz, solid line), microwave (15.4 GHz, dash–dotted line), hard X-ray (> 25 keV count rate, dashed histogram) and soft X–ray (3 – 25 keV, long dashed line) data for the flare at 20:08 UT on 1991 June 13. The relatively high point–to–point dispersion in the 86 GHz data is believed to be real, and to be associated with the fact that the radio source is somewhat larger than the maximum size to which the interferometer is sensitive. There is a very small enhancement in the 86 GHz flux associated with the main impulsive phase seen in hard X–rays and microwaves.

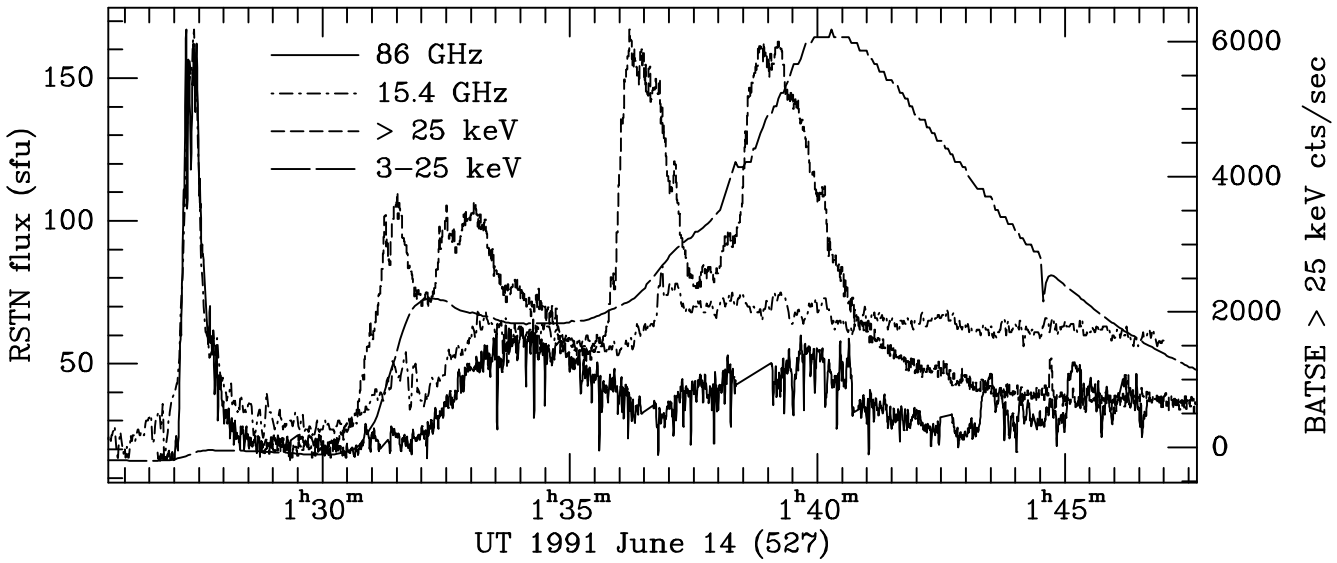

Figure 8. The millimeter (86 GHz, solid line), microwave (15.4 GHz, dash–dotted line), hard X-ray (> 25 keV count rate, dashed histogram) and soft X–ray (3 – 25 keV, long dashed line) data for the flare at 01:27 UT on 1991 June 14. The hard X–ray data do not start until 01:29:50 when the *Compton GRO* satellite emerged from the Earth's shadow; however, note the very small rise in the GOES soft X–ray flux associated with the main impulsive phase seen at both radio wavelengths.

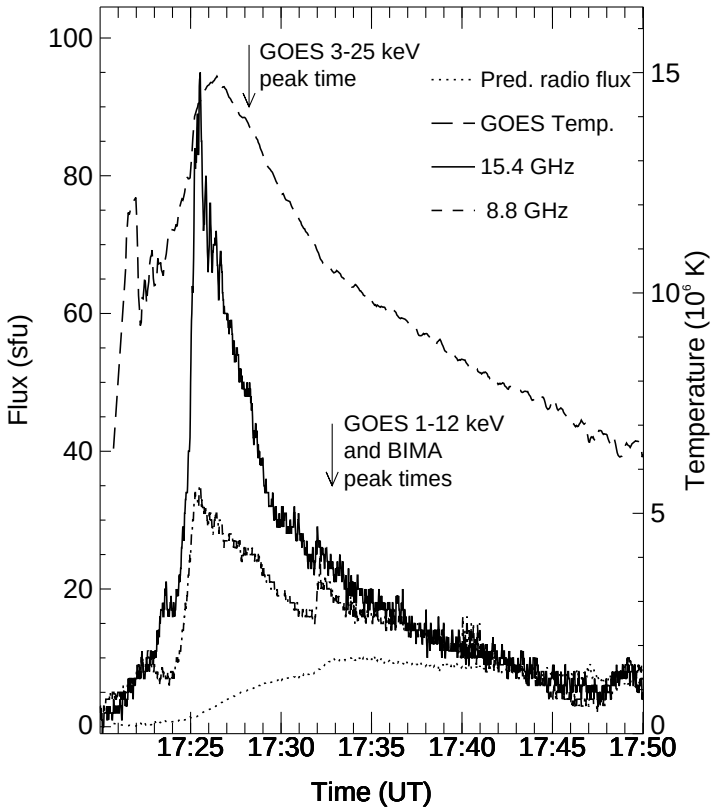

Figure 9. The temperature of the GOES material (long dashed line, axis to right of plot in units of 10^6 K) and the radio flux predicted at high frequencies (dotted line, axis to left of plot in sfu) for event 3 (1991 June 11 at 17:25 UT), based on free–free emission by an optically–thin source with the emission measure and temperature of the GOES material. For comparison we plot the observed RSTN microwave data at 15.4 GHz (solid line) and 8.8 GHz (dash–dotted line). The two arrows denote the times of the peaks in the GOES 3 – 25 keV channel (earliest arrow) and the 86 GHz data and the GOES 1.5 – 12 keV channel (coincident, second arrow).